Received: 05 January 2024 | Revised: 27 February 2024 | Accepted: 14 March 2024

https://doi.org/10.56946/jce.v3i1.298

Journal of Chemistry and Environment

Research Article

0D-3D Superstructure of Biocarbon with $FeCl_3$-Assisted for Electrochemical Symmetrical Supercapacitor

Sri Ayunda, Rakhmawati Farma*, Aria Yunita, Irma Apriyani

Department of Physics, University of Riau, Simpang Baru, Riau 28293, Indonesia, Indonesia.

*Correspondence:

rakhmawati.farma@lecturer.unri.ac.id

Abstract

Biomass materials exhibit a diversity of macrostructures that can be derived or developed into various 0D-3D nanoscale structural designs with various different dimensions such as spherical, nanofiber, tubular, nanosheet, hierarchical, nanosphere, and honeycomb structures, when converted into activated carbon. This research converts oil palm empty fruit bunch fiber biomass into supercapacitor carbon material by optimizing the chemical activation process by varying the activating reagent. The active carbon conversion process includes precarbonization stages, chemical activation (KOH, $FeCl_3$, and $ZnCl_2$), carbonization, and physical activation. The resulting electrode was confirmed to have a morphology with a 0D to 3D structure (nanosphere, nanofiber and nanopore) due to the $FeCl_3$ activator, so the resulting surface area was high (517.998 m/g). Biomass was successfully converted into carbon which was confirmed through through the resulting physical and electrochemical properties. The electrochemical performance of the sample supercapacitor cell was analyzed in a symmetric two-electrode system in 1 M H_2SO_4 electrolyte solution. The $FeCl_3$-activated samples shows the highest specific capacitance of 256 F/g at a scan rate of 1 mV/s. In addition, oil palm empty fruit bunch fiber biomass is a potential raw material, as a carbon material for supercapacitor cells with high performance.

Keywords: Nanostructured, 0-3D, chemical activation, biomass, supercapacitor

1. Introduction

Electrical energy has become a basic need for the world community and has had a major influence on almost all sectors of life. Energy needs that still depend on fossil fuels such as oil, coal, and natural gas as a source of electrical energy have had an impact on air pollution and will have an impact on the quality of life and health [1]. Energy demand also continues to increase along with economic activity in the industrial, transportation, commercial, and household sectors. The increasing need for energy encourages the presence of various alternative energies in solving the problem of the global energy crisis [2]. Electrical energy can be generated from renewable energy sources such as solar and wind, but the effectiveness of its use requires efficient storage of electrical energy. Developments in electrical energy storage systems are very important for generalizing the effectiveness of natural cycles of energy sources [3].

Supercapacitors (SCs) an energy storage devices, its use have the advantages of high superpower, long cycle life, fast charge-discharge rate, and resistance to high temperatures. Based on the energy storage mechanism, supercapacitors are divided into electrode double-layer capacitors (EDLC) and pseudocapacitors [4]. Three types of supercapacitors are widely used, namely double layer capacitors (EDLC), pseudocapacitors, and hybrid. The energy storage mechanism

in the EDLC type does not involve a faradaic reaction process because the capacitance comes from adsorbed ions. In the pseudocapacitor type, the capacitance is formed due to faradaic processes such as redox reactions and the hybrid type combines the properties of EDLC and pseudocapacitor [5]. EDLC supercapacitors consist of several material arrangements including electrodes, current collectors, electrolytes, and separators. Electrodes are very important devices in supercapacitor-based energy storage media because they can react directly to electrolytes. The main materials commonly used in the manufacture of supercapacitor electrodes include activated carbon, conducting polymers, metal oxides, graphene, and carbon nanotubes [6]. The electrode material from activated carbon is still the choice when compared to other materials because the availability of this type of material is still easy to obtain, does not require expensive costs, and has a high surface area, good electrical conductivity, and high electrochemical stability [7]. Utilizing activated carbon as a supercapacitor electrode will help solve problems from biomass waste, such as the conversion of biomass into activated carbon material. The biomass used to make supercapacitor materials must be of good biomass and can be found in the environment. Carbon materials obtained from biomass have advantages including abundant availability, low cost, renewable and environmentally friendly [8]. Currently, almost all types of biomass derived from plants, animals, and microorganisms are widely used as practical precursors for producing carbon materials [9].

The porous structure inherent in biomass as a raw material for supercapacitors will provide carbon products with suitable surface area (SSA) and high porosity. Researchers have developed many carbon materials that can induce superstructures of zero-dimensional (0D) (nanosphere), one-dimensional (1D) (nanofiber), two-dimensional (2D) (nanosheet), and three-dimensional (3D) (porous framework). Carbon materials with a 0D-3D porous structure can be produced from proper and appropriate treatment. The 0D-3D porous carbon structure is useful in penetrating electrolytes and ion diffusion for electrochemical performance in supercapacitors. Researchers [10] produced carbon material from empty palm fruit bunches with a 1D superstructure (nanofiber), having a specific capacitance of 201 F/g. Researchers [11] also produced carbon electrodes from date palm fronds with a 3D superstructure (honeycomb), having a specific capacitance of 227 F/g. Researchers [12] produced activated carbon made from orange peel with a 2D superstructure (nanosheet), having a specific capacitance of 289 F/g. Researchers [13] also produced activated carbon made from Zanthoxylum leaves with a 2D superstructure (nanosheet), having a specific capacitance of 160 F/g. Researchers [14] produced a 0D superstructure (nanosphere) using Cassia fistula shell biomass with a specific capacitance reaching 154 F/g. In this research, a 1D superstructure (nanofiber) was produced using OEF biomass with a specific capacitance reaching 256 F/g.

Oil palm empty bunches of fiber (OEF) are one of the solid wastes produced by the Oil palm processing industry. This unprocessed waste emits an unpleasant odor and becomes a breeding ground for flies, thus becoming waste that pollutes the environment and spreads pathogenic bacteria. OEF is a solid waste product from processing 22-23% of fresh fruit bunches (FFB). The organic material of OEF contains 22.60% lignin, 45.80% cellulose, 71.80% hemicellulose, 25.90% pentose, and 1.60% ash. The high lignocellulose content in empty oil palm fruit bunches can be processed as active carbon [15]. In this research, OEF was used as raw material for making active carbon. Activated carbon is activated using potassium hydroxide (KOH), ferric chloride ($FeCl_3$), and zinc chloride ($NiCl_2$) to obtain large capacitance. Activated carbon that has been activated is studied for its performance as a supercapacitor electrode by determining the characteristics of the activated carbon material and the resulting electrochemical properties.

Researchers [17] have made activated carbon from empty oil palm fruit bunch biomass which produces a morphology with a porous network structure (3D) and has a specific capacitance of 103.43 F g^{-1}. In this research, activated carbon based on empty oil palm fruit bunches was made which was activated

using potassium hydroxide (KOH), ferric chloride ($FeCl_3$), and zinc chloride ($NiCl_2$) to obtain a 0-3D structure and large capacitance. The performance of activated carbon that has been activated is studied as a supercapacitor electrode by determining the characteristics of the activated carbon material and the resulting electrochemical properties. OEF activated with $FeCl_3$ activator produces a morphology with a 0-3D superstructure (0D nanosphere, 1D nanofiber, and 3D nanopore) with a specific surface area of 517.998 m^2/g and a specific capacitance reaching 256 F/g.

2. Experiment

2.1 OEF conversion as a supercapacitor cell electrode

The process of converting Oil palm Empty bunches Fiber (OEF) into activated carbon is shown in Figure 1. First, the OEF is cleaned, and the fiber is separated from the outer skin of the OEF and dried in the hot sun. The pre-carbonization process was carried out to produce self-adhering powder at a temperature of 200◦C for 1 hour. Second, the powder obtained was activated by KOH, $FeCl_3$, and $ZnCl_2$ to induce the formation of a 0D-1D pore structure. OEF carbon powder was dispersed in 200 mL of distilled water at a temperature of 80 ℃ for 2 hours. The activated powder is converted into carbon pellets using a hydraulic press. Third, the carbon pellets are continuously carbonized-physically activated, respectively at a temperature of 600 ◦C for 1 hour with a heating rate of 3◦C min^{-1} under a flow of nitrogen gas and at a temperature of 800 ◦C for 1 hour with a heating rate of 10 ◦C min^{-1} under carbon dioxide gas flow. The carbon electrode obtained was soaked in distilled water until it reached a pH of ~7 and dried at 100◦C for 24 hours to obtain porous carbon. Carbon electrodes based on KOH, $FeCl_3$, and $ZnCL_2$ activation are coded respectively OEF-K, OEF-F, and OEF-Z. The carbon electrode that will be applied to the supercapacitor cell is polished until it is shaped like a coin with a diameter of 0.7 mm and a thickness of 0.2 mm, then immersed in a 1 M H_2SO_4 electrolyte solution.

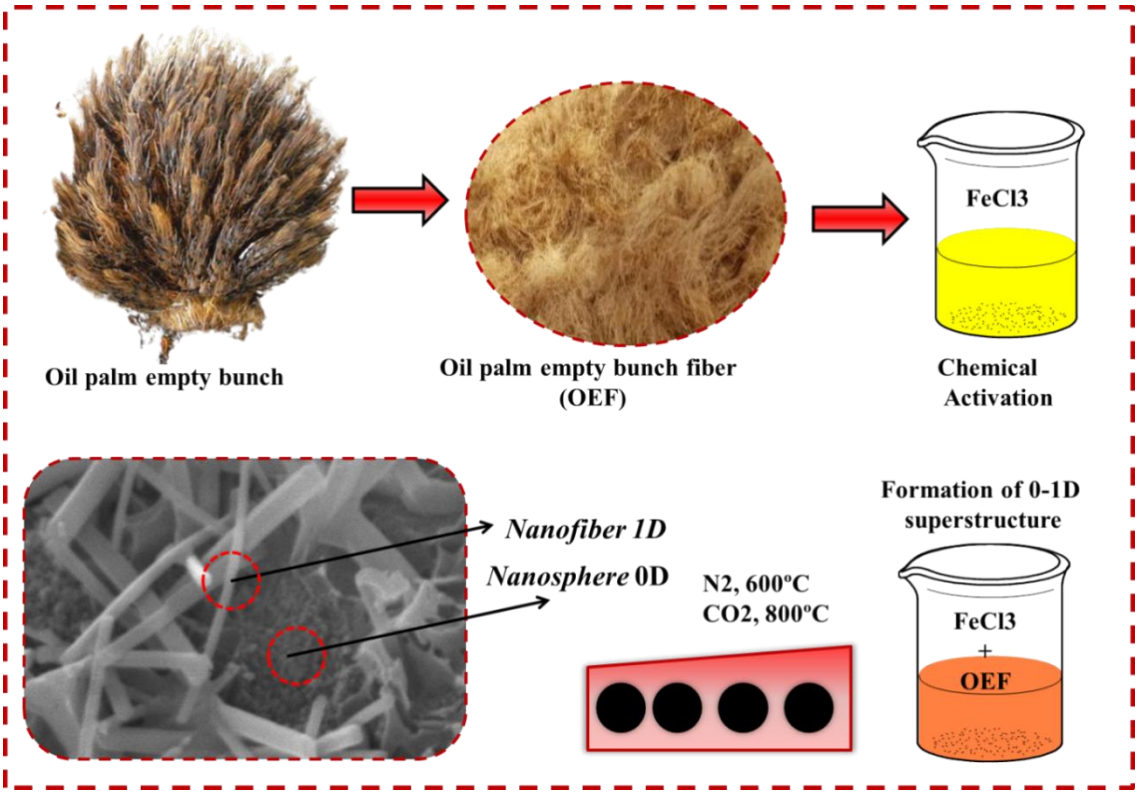

Figure 1. Process of converting OEF to activated carbon.

2.2 Characterization and Measurements of Electrochemical

X-ray Diffraction characterization was carried out to determine the microcrystalline structure of activated carbon using an X'pert instrument with an X-Pert Powder Panalytical type system, which uses a Cu K-α light source, with a wavelength of 15.406 nm at a diffraction angle of 2θ, 10˚- 60 ˚. Fourier Transform Infrared characterization was carried out to determine the functional groups of activated carbon using the Shimadzu IRPrestige-21 instrument at wave numbers 450-4500. Furthermore, to determine the surface morphology, a scanning electron microscopy (SEM) characterization was carried out and the chemical content was carried out and Energy Dispersive X-ray (EDX) characterization using the SEM-EDX, JEOL JSM-6510 LA instrumentation. The surface area and pore distribution were also analyzed using the N_2 isothermal adsorption-desorption method using the respective characterizations of Brunauer-Emmett-Teller (BET) and Barrett-Joyner-Halenda (BJH) with the Quantachrome TouchWin v1.22 (St 3 on NOVA touch). 4LX) instrument. The electrochemical measurements were carried out in a symmetrical two-electrode system under 1 M H2SO4, where they were separated by a hen eggshell membrane. Electrochemical measurements using the first method using Cyclic Voltammetry on a two-electrode system in 1 M H2SO4 solution as an electrolyte solution with a scan rate of 1-10 mV/s at a potential difference of 0-1V. Second, using a Galvanostatic Charge Discharge at a potential of 0-1 V with a current density of 1-10 A/g at a potential difference of 0-1V. The CV-GCD test uses the CV-GCD UR Rad-Far 5841 Physics instrument.

3. Results and Discussion

3.1 Morphological and Constituent analysis of OEF samples

Micrographs of OEF samples were identified using SEM analysis with optimization of the chemical activation process. Figure 2 shows the results of micrographs in the form of surface morphology which has various shapes based on the induction of the activating agent. Figures 2 (a) and (b) show the surface morphology of the OEF-K sample which has aggregates and several interconnected pores. This is because the KOH activator cannot react with the lignocellulose found in OEF biomass in a complex manner, this reaction only evaporates a small portion of the oxygen and hydrogen from the lignin, cellulose, and hemicellose compounds, so there are still impurities that fill the carbon matrix and form aggregates. Some decomposing lignocellulosic compounds will leave pore wells, forming several interconnected pores. Figures 2(c) and (d) show the surface morphology of the OEF-F sample, which has nanosphere, nanofiber, and nanopore structures. The role of $FeCl_3$ in the formation of nanofibers is that $FeCl_3$ reacts with the cellulose compound $C_6H_{10}O_5$, this reaction decomposes and evaporates cellulose to form nano-sized fibers. Cellulose is composed of interconnected microfibrils and can be converted into nanofibrils by $FeCl_3$. Furthermore, $FeCl_3$ can also evaporate and decompose lignin and hemicellulose to form nanopores and nanosphere. The $ZnCL_2$ activating agent is also able to evaporate and decompose cellulose compounds to form nanofiber structures, but the resulting nanofibers have a larger diameter (Figure 2 (e) and (f)).

The results of SEM analysis confirm that the activating agent has a major influence on the formation of the superstructure of the carbon electrode material. The 0D nanosphere structure can provide and ensure that ions can diffuse across the wall for the charge and discharge process [11]. The nanosphere structure will also feature special improvements such as excellent elasticity, compressibility, and recoverability. In addition, the superstructure also provides low resistance channels as a reservoir for electrolyte ions which will facilitate energy storage and can withstand high current loads and increase the electroactive surface area [19]. The nanofiber structure also called 1D superstructure on carbon electrodes can be a medium or access for rapid diffusion of electrolyte ions, resulting in a high bilayer charge along with increasing the performance of supercapacitor cells [16]. In addition, the pore wells formed are associated with a 3D superstructure which is useful as a medium for diffusion and storage of

electrolyte ions. In the OEF-F SEM results, a nanosphere structure is also formed which will provide special improvements such as excellent elasticity, compressibility, and recoverability. Apart from that, the upper building also provides a low resistance channel as a reservoir for electrolyte ions which will facilitate energy storage and can withstand high current loads and increase the electroactive surface area [17].

Energy Dispersive X-ray analysis was used to analyze the chemical content of the OEF carbon electrode. In general, all OEF samples contain the elements carbon (C), oxygen (O), magnesium (Mg), and silica (Si). The element Chlorine (Cl) is only found in samples OEF-F and OEF-Z and the element Zinc (Zn) is only found in OEF-Z. Figure 3 shows that the OEF biomass-based carbon electrode element is dominated by carbon elements with the highest mass percentage, namely 80.86%. The high carbon content is caused by the use of OEF biomass as a carbon source for electrode material. Carbon derived from OEF can be a renewable and environmentally friendly alternative [18].

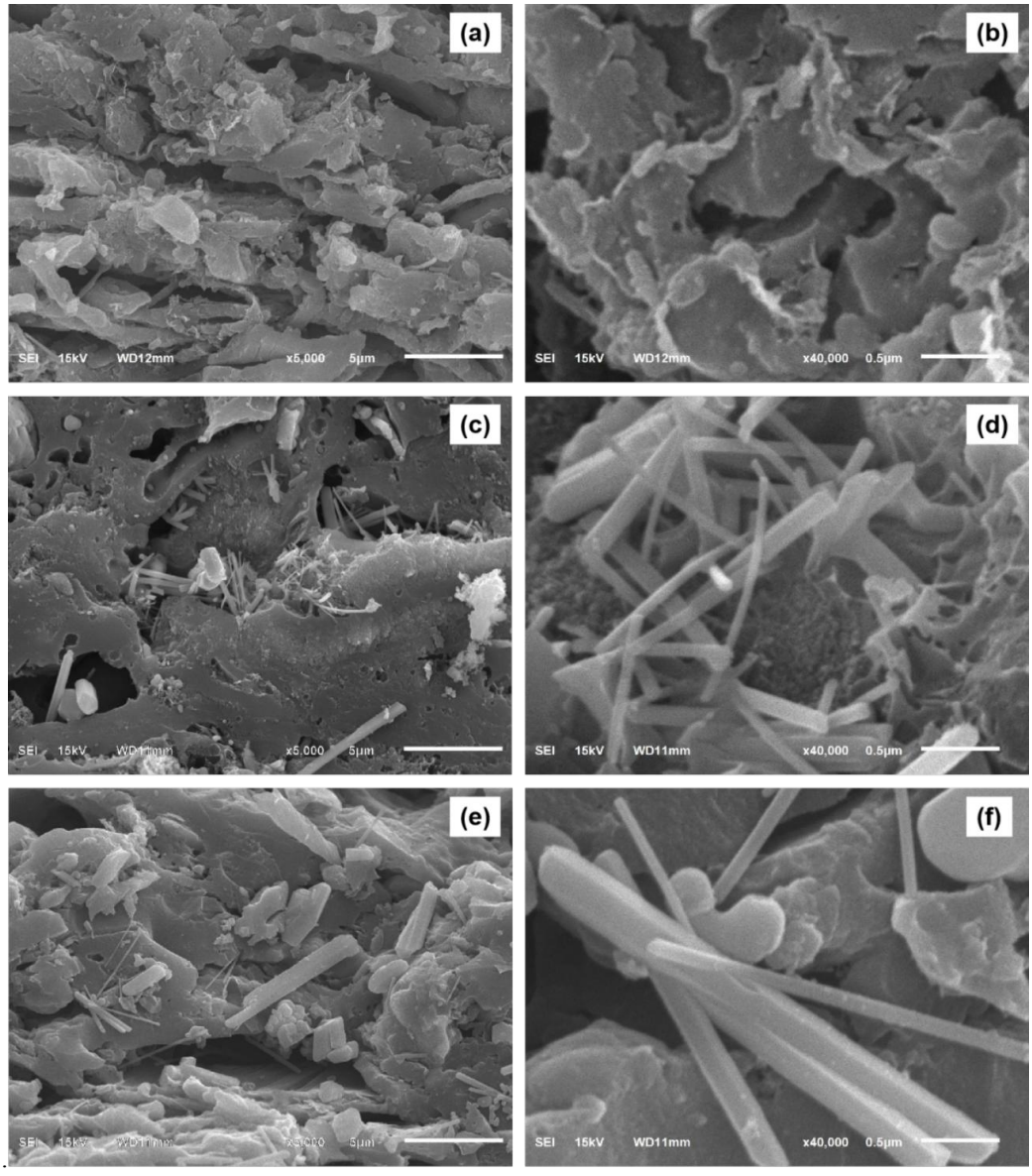

Figure 2: Image of surface morphology (a) OEF-K (5000x), (b) OEF-K (40,000x), (c) OEF-F (5000x), (d) OEF-F (40,000x), (e) OEF-Z (5000x), (f) OEF-Z (40,000x)

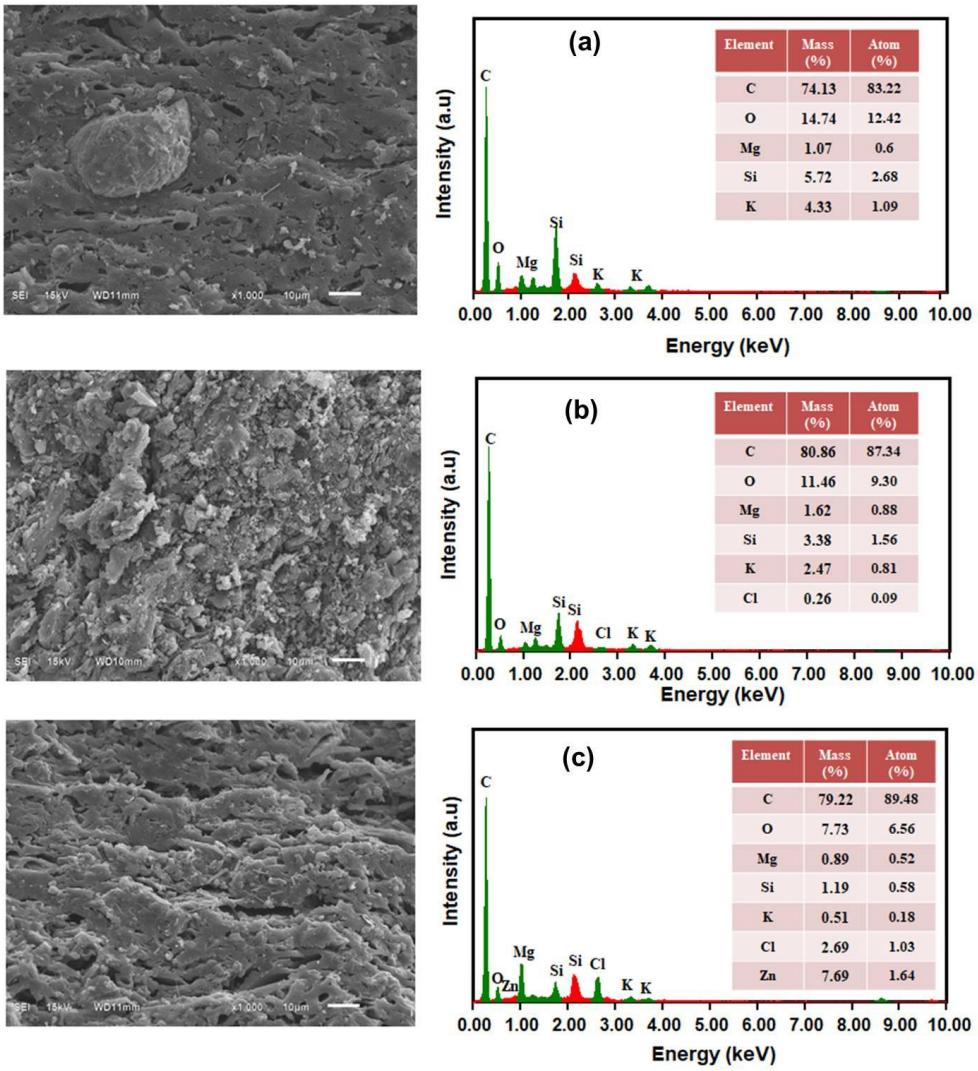

Figure 3. EDX result curve (a) OEF-K (b) OEF-F (c) OEF-Z

3.2 Analysis of the physical properties of the OEF electrode

The microcrystalline structure of the OEF electrode with optimized chemical activation was analyzed using the XRD method. Figure 4 (a) displays the diffraction pattern of the entire sample with the presence of two sloping peaks at 2θ = 24° and 45° which correspond to the (002) and (001) lattice planes. The two sloping peaks indicate that the sample has an amorphous carbon structure which usually results from the carbonization process - physical activation [19]. The sample activated with KOH (OEF-K) has several sharp peaks at angles 2θ = 23°, 35°, 47° and 56° which indicate the presence of a calcium carbonate ($CaCO_3$) crystal structure. This compound comes from the OEF biomass structure which is not completely decomposed in the carbon electrode fabrication process [20]. In samples activated with $ZnCl_2$ activator (OEF-Z), several crystalline compounds were detected such as silicon dioxide (SiO_2) at angles 2θ = 27° and 29°, zinc oxide (ZnO) compounds at angles 2θ = 34° and 36°, and compounds $CaCO_3$ at an angle of 2θ = 56° [21] [22]. The ZnO compound comes from the reaction between $ZnCl_2$ and lignocellulose found in OEF biomass, while $CaCO_3$ and SiO_2 are compounds originating from OEF biomass [23]. These compounds are formed because the carbon electrode washing process is less than optimal and these compounds are not completely decomposed in the physical carbonization-activation process. Meanwhile, in the sample with the active ingredient $FeCl_3$ (OEF-F), one peak was observed at an angle of 2θ = 43.1°, indicating the presence of a Fe_3O_4 structure.

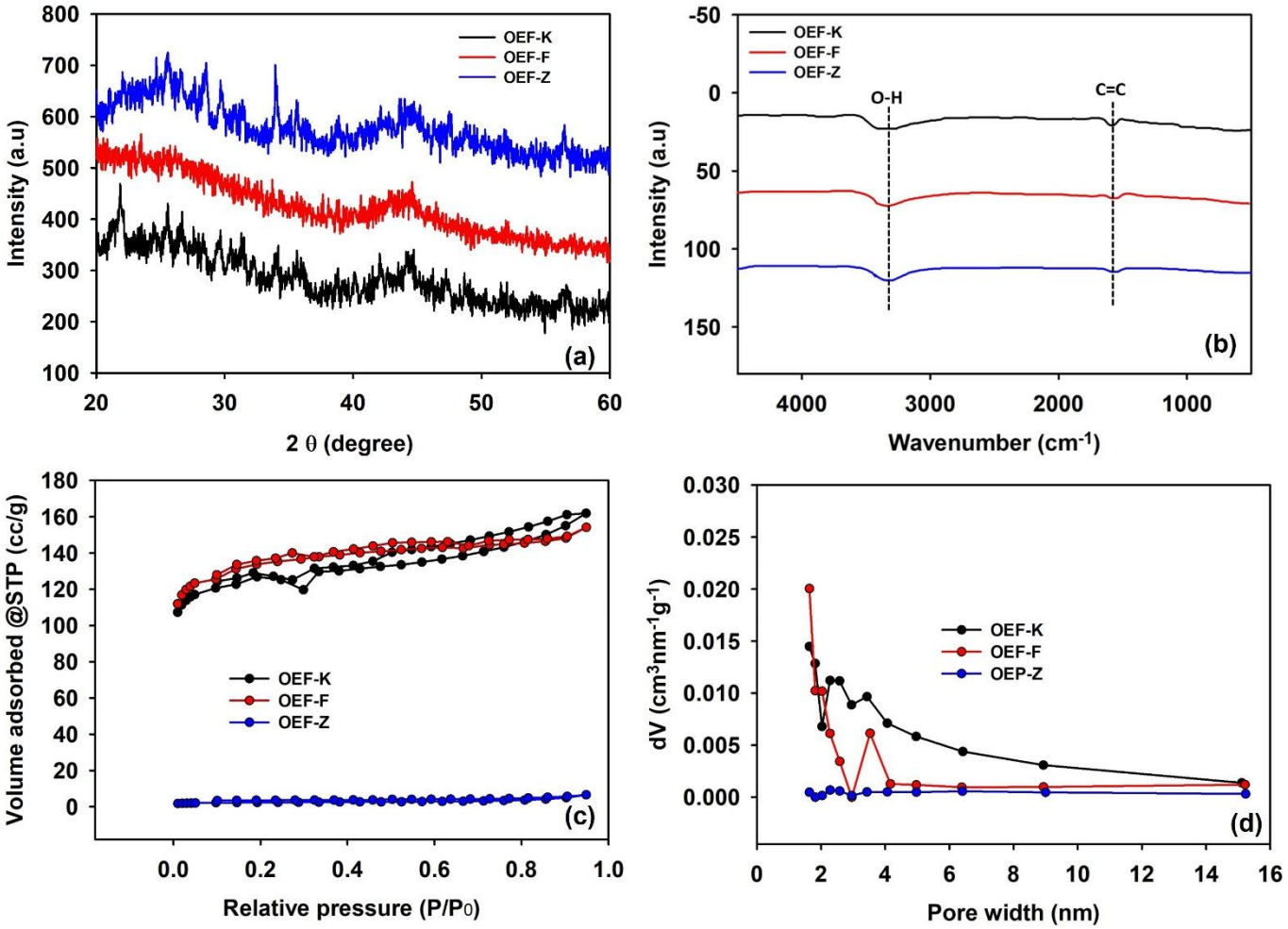

Figure 4: (a) XRD pattern, (b) FTIR spectrum, (c) N2 adsorption/desorption isotherms, and (d) Pore size distribution curves OEF samples with varying activators

The presence of Fe_3O_4 is caused by the activating agent $FeCl_3$ reacting with CO_2 at high temperatures (carbonization - physical activation process) so that most of the Fe is lost and reduced to Fe_3O_4. This phenomenon has an impact on the physical properties of the carbon electrode, where the Fe_3O_4 compound in the carbon matrix causes magnetic properties that can affect ion transport when the sample is in the electrolyte [24]. Based on research by Zhang et al [25], when an electrode containing a magnetic field is dipped into the H_2SO_4 electrolyte, it will provide a driving force caused by the Lorentz force which can have a positive influence in accelerating ion transport. In addition, the OEF-F sample has a steeper peak than the other two samples, indicating that it has higher amorphous properties. The amorphous nature or high disorder can increase ion mobility so that it has better conductivity [26].

Figure 4 (b) shows the FTIR spectra of samples prepared with different pegactive agents recorded at absorptions of 4500 – 500 cm^{-1}. The OEF-K, OEF-F, and OEF-Z samples have absorption peaks in adjacent bands. The OEF-K sample shows spectrum peaks in the 3400 cm^{-1} and 1500 cm^{-1} bands [27]. The OEF sample with $FeCl_3$ activator (OEF-F) has characteristic vibration bands at 3420 cm^{-1} and 1550 cm^{-1} [28]. The OEF-Z sample shows peaks at 3440 cm^{-1} and 1553 cm^{-1} [29]. The band at 3600 – 3200 cm^{-1} comes from the –OH bond vibration of the hydroxyl group [27]. The characteristics of the band around 1550 cm^{-1} are related to the C=C strain vibrations in the aromatic ring [24]. Activated carbon which has

hydroxyl functional groups can form bonds with carbon on the electrode surface, helping in the formation of complex pore structures. This increases the effective surface area of the electrode, thereby increasing the energy storage capacity of the supercapacitor cell. Furthermore, hydroxyl can increase the electrode's ability to be immersed in electrolyte, increasing surface wettability, so that electrode-electrolyte ion exchange occurs efficiently [1]. The C=C functional group indicates the presence of carbon purification so that the resulting conductivity is high [30].

Samples OEF-K, OEF-F, and OEF-Z were further characterized to determine their specific surface area and porosity using the N_2 adsorption-desorption method. Figure 4 (c) shows the isotherm curve of the OEF sample which forms a type IV isotherm pattern based on the IUPAC classification due to the presence of microporous and mesoporous structures in the resulting carbon material [31]. Based on this curve, it can be seen that the adsorption volume and relative pressure have a linear relationship. When the pressure ratio is relatively high, the adsorption volume will increase slightly. Even though the isotherm patterns produced from the three samples are quite similar, it can be seen from the data that the volume of N_2 adsorption produced is different. This adsorption volume depends on the presence of a pore structure on the surface area of the activated carbon [32]. Apart from that, the hysteresis loop formed also varies according to the activating material used. The formation of this hysteresis loop is due to the presence of adsorbed N_2 gas and shows the large surface area that will be obtained [1].

The OEF-Z sample displays the lowest N_2 adsorption volume and the hysteresis loop formed is not very obvious. This shows that the sample has a poor pore structure because hysteresis shows that the pores are in the shape of a narrow ink bottle, resulting in the pores being narrowed and the mesopores and micropores being formed imperfectly [15]. The OEF-K sample shows increased N_2 adsorption volume and has an H4-type hysteresis loop which implies the presence of micropores and mesopores in the sample. The OEF-F sample also shows a type IV isotherm pattern with an H4 hysteresis loop, but the adsorption volume is larger than OEF-K. This can show that the OEF-F sample has a high microporous and mesoporous structure so the resulting surface area is high [33].

The specific surface areas of samples OEF-K, OEF-F, and OEF-Z are 490.881, 517.998, and 8.854 m^2/g, respectively. The difference in the specific surface area produced is of course caused by the active material used. The highest specific surface area is owned by the OEF-F sample, this is because the $FeCl_3$ activating agent can. induce 0-1 D superstructures, namely nanospheres and nanofibers, which are confirmed in SEM analysis. The pore size distribution consisting of micropores and mesopores throughout the sample can be confirmed through the pore size distribution plot as shown in Figure 4 (d). The pore size distribution is in the range < 2 nm which indicates the presence of a microporous structure and in the range 2 - 15.8 nm indicates the presence of a mesoporous structure in the carbon matrix [34]. In general, the mesoporous structure plays a role in diffusing electrolyte ions and micropores will store these ions in carbon materials so that they can increase the supercapacitive properties of supercapacitor cells [35].

3.3 Supercapacitor measurement by two-electrode system

Further exploration of the OEF samples was carried out by testing the electrochemical properties in a two-electrode configuration in a 1 M H_2SO_4 electrolyte solution using CV and GCD. A comparison of CV curves from samples OEF-K, OEF-F, and OEF-Z is shown in Figure 5 (a). As can be seen in the figure, the curves of all samples have a quasi-rectangular shape which is a type of EDLC. The curve of the OEF-F sample has the largest curve area which shows that this sample has a higher charge-discharge rate with the highest specific capacitance value of 255 F g^{-1} [36]. The capacitive properties of the OEF-F sample are superior to other samples due to several factors. The dominant factor is that the OEF sample has a superstructure of 0D nanospheres, 1D nanofibers, and 3D nanopores which has been confirmed by SEM analysis. The 3D structure of supercapacitor cells plays an important role in storing electrolyte charge efficiently.

.

.

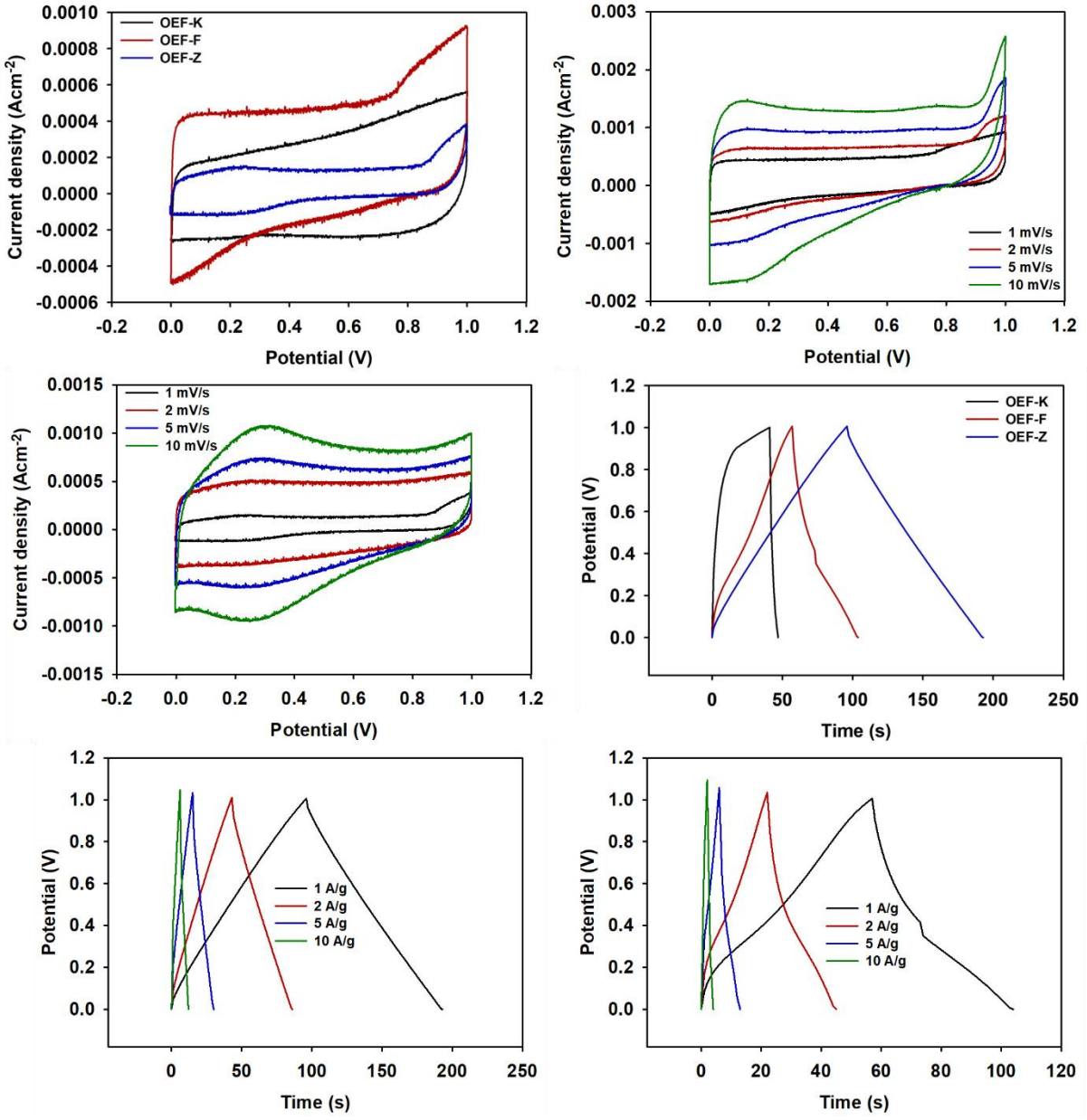

Figure 5: CV curve (a) OEF, (b) OEF-F, (c) OEF-Z, GCD curve (d) OEF, (e) OEF-Z, and (f) OEF-F

The larger surface area is due to the availability of additional space in the third dimension, which allows an increased amount of electrolyte to be stored in the supercapacitor cell. In addition, the 3D structure can also be a more efficient conductive path for ions to move, speeding up the charging and discharging process of supercapacitor cells. Thus, the performance of the 3D structure in storing the electrolyte charge not only enlarges the cell capacity but also improves the overall efficiency and performance of the supercapacitor cell [30].

The 2D nanofiber structure can create space for electrode-electrolyte interactions, while the nanopores facilitate ion diffusion in the electrolyte, resulting in high charge storage capacity and fast ion accessibility, which supports the

performance of supercapacitors with large energy absorption capacity and fast charging time. Nanospherical structures have a crucial role in storing electrolyte charge in supercapacitor cells [1]. The nanospherical shape provides advantages in terms of uniform volume and high surface area. The large surface area enables intense interactions between the nanospherical and the electrolyte, thereby increasing the charge storage capacity. In addition, this spherical structure also facilitates the efficient movement of electrolyte ions around its surface, which is important for achieving fast charge and discharge performance [37].

This combination of superstructures can produce a greater amount of bilayer charge and can create supercapasitive properties that are superior to other samples. Furthermore, OEF samples also have better amorphous properties and higher specific surface area [38]. The OEF-K sample has a specific capacitance value of 128 F g^{-1} and the OEF-Z sample has the lowest specific capacitance value of 80 F g^{-1}. Figures 5 (b) and (c) display the CV curves of the OEF-Z and OEF-F samples with scan rates of 1, 2, 5, and 10 mV/s. The curve formed still maintains its quasi-rectangular shape even though the scanning rate used is high, this indicates that OEF-activated carbon has good capacitive characteristics [39].

GCD measurements were carried out to evaluate the performance of OEF further activated carbon with various activators. As shown in Figure 5 (d), the GCD curves of all samples are isosceles triangles indicating EDLC behavior. OEF-F has the largest curve, meaning this sample has high charge-discharge efficiency and good reversibility in the charge and discharge process. In addition, the longer discharge time reflects a larger sample-specific capacitance which is by the CV analysis [40]. Figures 5 (e) and (f) show the GCD curve with an increase in current density of 1 to 10 A/g from the ZnCl and $FeCl_3$ samples respectively. From the curve, it can be seen that the lower the current density, the longer the charging time required so that the curve formed is larger and the specific capacitance value produced is higher. This happens because the lower the current density, the more areas the ions will pass through and the longer the time required for the ions to diffuse [33]. Table 1 presents a comparison of the electrochemical performance of biomass-based supercapacitor cell active materials with different chemical activating agents.

Table 1: Comparison of activator, superstructure, SSA, Csp, Wsp, and Psp from various biomasses for supercapacitor cell carbon materials.

Biomass	Activator	Superstructure	SSA (m^2 g^{-1})	C_{sp} (F g^{-1})	Reference
Bamboo	NaOH	honeycomb	1128	280	[41]
Ficus macrocapa roots	$KHCO_3$	honeycomb	1454.7	220	[42]
sugar cane stalks	KOH	hirarkis	3178	198.4	[43]
Cassia fistula shell	NH_3	nanosphere	1915	154	[14]
Spirulina peel	KOH	tubular	122	222.7	[44]
Orange peel	H_3PO_4	nanosheet	-	289	[45]
Cotton seed	K_2CO_3	nanosheet	2361	313	[46]
Zanthoxylum leaves	$ZnCl_2$	nanosheet	1242	160	[13]
Empty bunches of sugar palm	KOH	nanofiber	1231	201	[10]
Oil palm emptybunchess fiber	KOH	-	490.881	128	This work
Oil palm emptybunchess fiber	$FeCl_3$	nanofiber and nanosphere	517.998	256	This work
Oil palm emptybunchess fiber	ZnCl	nanofiber	8.854	80	This work

4. CONCLUSION

In this work, carbon materials activated using KOH, $FeCl_3$, and

$ZnCl_2$ have been developed from Oil palm Empty bunches of Fiber biomass using a two-step pyrolysis process. The optimized OEF supercapacitor cell carbon electrode can produce 0-3D nanostructures, providing space for charge storage and accelerating electrolyte ion kinetics from the activating regen cooperative effect. Based on porosity analysis, the sample has a microporous (<2 nm) and mesoporous (2 - 15.8 nm) structure, and a specific surface area of 517.998 m^2/g In addition, OEF also has an amorphous structure and shows a high specific capacitance of 256 F/g at 1 mV/s in a two-electrode system. It was concluded that activated carbon derived from oil palm bunches induced by $FeCl_3$ has the potential to be used as an electrode for energy storage devices that is economical, renewable, and sustainable.

Authors Contribution

Sri Ayunda: Methodology and Conceptualization. Rakhmawati Farma: Investigation, Validation, Supervision, Writing-original draft, Visualization. Aria Yunita: Writing-original draft, Formal analysis. Irma Apriyani: Conceptualization, Project administration, writing original draft, review, and editing.

Conflicts of Interest

The authors declare that they have no known competing financial interests or personal relationships that could have appeared to influence the work reported in this paper.

Acknowledgment

The authors are grateful to the DRPM Kemenristek/BRIN, Republic of Indonesia for financial support through the first-year project of Penelitian Tesis Magister (PTM), with contract number: 15490/UN.19.5.1.3/AL.04/2023.

Data Availability statement

The data presented in this study are available on request from the corresponding author.

Funding. This study was supported by Penelitian Tesis Magister (PTM) (15490/UN.19.5.1.3/AL.04/2023).

REFERENCES

1. Farma, R., et al., Enhanced electrochemical performance of oxygen , nitrogen , and sulfur trial-doped Nypa fruticans -based carbon nanofiber for high performance supercapacitors. Journal of Energy Storage, 2023. 67. p. 1-11.
2. Li, L. et al. Formamide hydrothermal pretreatment assisted camellia shell for upgrading to N-containing chemical and supercapacitor electrode preparation using the residue. Energy, 2023. 265. p.126247.
3. Yan, B. et al. Applied Surface Science Nitrogen-doped carbon layer on cellulose derived free-standing carbon paper for high-rate supercapacitors. Applied Surface Science, 2023. 608. p. 155144.
4. Geng, X. et al. Biomass derived nanoarchitectonics of porous carbon with tunable oxygen functionalities and hierarchical structures and their superior performance in CO2 adsorption and energy storage. Carbon, 2023. 214. p. 118347.
5. Ahmad, F. et al. Advances in graphene-based electrode materials for high-performance supercapacitors: A review. Journal of Energy Storage, 2023. 72. p. 108731.
6. Xue, B., Xu, J. & Xiao, R. Ice template-assisting activation strategy to prepare biomass-derived porous carbon cages for high-performance Zn-ion hybrid supercapacitors. 2023. 454.
7. Thirumal, V. et al. Characterization of activated biomass carbon from tea leaf for supercapacitor applications. Chemosphere, 2022. 291. p. 132931.
8. Bi, R., Pang, S. K., Yung, K. C. & Yin, L. K. Comprehensive study of used cigarette filters-derived porous activated carbon for Supercapacitors: From biomass waste to sustainable energy source. Journal of Electroanalytical Chemistry, 2022. 925. p. 116915.
9. Saka, T. et al. Evaluation of the Physical Properties of Various Biomass Materials for the Production of Activated Carbon. Journal of Chemistry and Environment, 2023. p. 30–39.
10. Farma, R., Apriyani, I., Awitdrus, A., Taer, E. & Apriwandi, A. Hemicellulosa-derived Arenga pinnata bunches as free-standing carbon nanofiber membranes for electrode material supercapacitors. Scientific Reports, 2022. 12. p. 1–11.
11. Farma, R. et al. Honeycomb-Like Carbon with Tunable Pore Size from Biomass Phoenix Dactylifera Midrib for Highly Compressible Binder-Free Supercapacitors. JOM, 2023.
12. Jia, B., Mian, Q., Wu, D. & Wang, T. Heteroatoms self-doped porous carbon from cottonseed meal using K2CO3 as activator and DES electrolyte for supercapacitor with high energy density. Materials Today Chemistry, 2022. 24.
13. Xu, Y. et al. Three-dimensional zanthoxylum Leaves-Derived nitrogen-Doped porous carbon frameworks for aqueous supercapacitor with high specific energy. Journal of Energy Storage, 2020. 32.
14. Young, C. & Chen, H. T. Supercapacitor application of a three-dimensional carbon sphere–intercalated porous carbon fabricated using a hard template and a biomass material. Diamond and Related Materials, 2022. 130. p. 109528.
15. Ayinla, R. T. et al. A review of technical advances of recent palm bio-waste conversion to activated carbon for energy storage. Journal of Cleaner Production, 2019. 229. p. 1427–1442.
16. Manasa, P., Sambasivam, S. & Ran, F. Recent progress on

biomass waste derived activated carbon electrode materials for supercapacitors applications—A review. Journal of Energy Storage, 2022. 54. p. 105290.
17. Zhang, S., Su, Y., Zhu, S., Zhang, H. & Zhang, Q. Effects of pretreatment and FeCl3 preload of rice husk on synthesis of magnetic carbon composites by pyrolysis for supercapacitor application. Journal of Analytical and Applied Pyrolysis, 2018. 135. p. 22–31.
18. Ghosh, S. et al. Natural biomass derived hard carbon and activated carbons as electrochemical supercapacitor electrodes. Scientific Reports, 2019. 9. p. 1–16.
19. Farma, R., Winalda, B. & Apriyani, I. The Self-Adhesive Properties of Carbon Activated-Like Shape Coin Derived From Palmae Plant Waste and Used as High-Performance Supercapacitor Electrodes. Journal of Electrochemical Energy Conversion and Storage, 2023. 20. p. 1–7.
20. Farma, R., Tania, Y. & Apriyani, I. Conversion of hazelnut seed shell biomass into porous activated carbon with KOH and CO2 activation for supercapacitors. Materials Today: Proceedings, 2023. p. 0–5.
21. Yunita, A., Farma, R., Awitdrus, A. & Apriyani, I. The effect of various electrolyte solutions on the electrochemical properties of the carbon electrodes of supercapacitor cells based on biomass waste. Materials Today: Proceedings, 2023.
22. Farma, R., Julita, R. I., Apriyani, I., Awitdrus, A. & Taer, E. ZnCl2-assisted synthesis of coffee bean bagasse-based activated carbon as a stable material for high-performance supercapacitors. Materials Today: Proceedings, 2023. p. 1–7.
23. He, G., Yan, G., Song, Y. & Wang, L. Biomass Juncus Derived Nitrogen-Doped Porous Carbon Materials for Supercapacitor and Oxygen Reduction Reaction. Frontiers in Chemistry, 2020. 8. p. 1–10.
24. Xu, Z. et al. Insights into the pyrolysis behavior and adsorption properties of activated carbon from waste cotton textiles by FeCl3-activation. Colloids and Surfaces A: Physicochemical and Engineering Aspects, 2019. 582. p. 123934.
25. Zhang, L. et al. Magnetic field-induced capacitance change in aqueous carbon-based supercapacitors. Cell Reports Physical Science, 2021. 2. p. 100455.
26. Zhang, J. et al. Amorphous Electrode: From Synthesis to Electrochemical Energy Storage. Energy and Environmental Materials, 2022. p. 1–28.
27. Padilla-Martínez, E. D., Pérez-Buendía, S. K., López-Sandoval, R. & Sánchez-Rodríguez, C. E. Electrochemical energy storage from spent coffee grounds-derived carbon by KOH activation. Journal of Energy Storage, 2023. 71. p. 108115.
28. Bedia, J., Peñas-Garzón, M., Gómez-Avilés, A., Rodriguez, J. J. & Belver, C. Review on Activated Carbons by Chemical Activation with FeCl3. C — Journal of Carbon Research, 2020. 6 (21).
29. Sujiono, E. H. et al. Fabrication and characterization of coconut shell activated carbon using variation chemical activation for wastewater treatment application. Results in Chemistry, 2022. 4. p. 100291.
30. Farma, R., Indriani, A. & Apriyani, I. Hierarchical-nanofiber structure of biomass-derived carbon framework with direct CO2 activation for symmetrical supercapacitor electrodes. Journal of Materials Science: Materials in Electronics, 2023. 34.
31. Zhang, S., Zhu, S., Zhang, H., Liu, X. & Xiong, Y. Synthesis and characterization of rice husk-based magnetic porous carbon by pyrolysis of pretreated rice husk with FeCl3 and ZnCl2. Journal of Analytical and Applied Pyrolysis, 2020. 147. p. 104806.
32. Borghei, S. A. et al. Synthesis of multi-application activated carbon from oak seeds by KOH activation for methylene blue adsorption and electrochemical supercapacitor electrode. Arabian Journal of Chemistry, 2021. 14. p. 102958.
33. Harahap, E. W., Taer, E., Rini, A. S., Taslim, R. & Apriwandi, A. Cassava peel derived self-doped and hierarchical porous carbon as an optimized electrode for the ultra-high energy density of supercapacitor. Diamond and Related Materials, 2022. 129. p. 109407.
34. Rustamaji, H., Prakoso, T., Devianto, H., Widiatmoko, P. & Adi, K. Bioresource Technology Reports Facile synthesis of N , S-modified activated carbon from biomass residue for promising supercapacitor electrode applications, 2023. 21.
35. Wang, H. et al. Micro-meso porous structured carbon nanofibers with ultra-high surface area and large supercapacitor electrode capacitance. Journal of Power Sources, 2021. 482. p. 228986.
36. Ye, R., Cai, J., Pan, Y., Qiao, X. & Sun, W. Microporous carbon from malva nut for supercapacitors: effects of primary carbonizations on structures and performances. Diamond and Related Materials. 2020. 105.
37. Farma, R., Putri, H. & Apriyani, I. KOH-assisted synthesis of oxygen-rich activated carbon derived from biomass sugar palm midrib as performance electrode cell supercapacitor. Energy Sources, Part A: Recovery, Utilization, and Environmental Effects, 2023. 45. p. 4886–4897.
38. Zhang, X. et al. Porous and graphitic structure optimization of biomass-based carbon materials from 0D to 3D for supercapacitors: A review. Chemical Engineering Journal, 2023. 460. p. 141607.
39. Farma, R., Yunita, A. & Apriyani, I. Diamond & Related Materials Addition of reduced graphene oxide to carbon shaft based on cerbera manghas mesocarp to improve energy storage performance of supercapacitor cells. Diamond & Related Materials, 2024. 143. p. 110922.
40. Cheng, Y. et al. Synthesis of porous carbon materials derived from laminaria japonica via simple carbonization and activation for supercapacitors. Journal of Materials Research and Technology, 2020. 9. p. 3261–3271.
41. Pang, X., Cao, M., Qin, J., Li, X. & Yang, X. Synthesis of bamboo-derived porous carbon: exploring structure change, pore formation and supercapacitor application. Journal of Porous Materials, 2022. 29. p. 559–569.
42. Wang, H. et al. Unveiling the cooperative roles of pyrrolic-N and carboxyl groups in biomass-derived hierarchical porous carbon nanosheets for high energy-

power Zn-ion hybrid supercapacitors. Applied Surface Science, 2022. 598. p. 153819.
43. Liu, H. et al. High energy-power zinc-ion hybrid supercapacitors achieved by 3D channels enriched biomass-derived N / O co-doped 2D arcuate carbon nanosheets, 2023. 29. p. 101476.
44. Ma, M. et al. 3D stack tubular mesoporous carbon derived from discarded sesame capsule shells for high-performance supercapacitors. Diamond & Related Materials, 2023. 131. p. 109562.
45. Gehrke, V. et al. Facile preparation of a novel biomass-derived H3PO4 and $Mn(NO_3)_2$ activated carbon from citrus bergamia peels for high-performance supercapacitors. Materials Today Communications, 2021. 26.
46. Jia, B., Mian, Q., Wu, D. & Wang, T. Heteroatoms self-doped porous carbon from cottonseed meal using K2CO3 as activator and DES electrolyte for supercapacitor with high energy density. *Materials Today Chemistry*, 2022. **24**. p. 100828.

How to cite this article:
Ayunda S,Farma R, Yunita A, Apriyani I. (2024). 0D-3D Superstructure of Biocarbon with FeCl3-Assisted for Electrochemical Symmetrical Supercapacitor. *Journal of Chemistry and Environment.* 3(1). p. 64-76

Authors bibliography

Sri Ayunda is a master's degree student from the University of Riau, Indonesia.

Rakhmawati Farma is a lecturer and professor as well as the secretary in the Department of Physics, Faculty of Mathematics and Natural Sciences, University of Riau, Indonesia. In addition, she also serves as coordinator of the Material Physics Laboratory at the University of Riau. Apart from being a lecturer, she is also active in research. Her research focuses on the technology of electrochemical energy storage, especially supercapacitor.

Aria Yunita is a master's degree student from the University of Riau, Indonesia.

Irma Apriyani is a master's degree student from the University of Riau, Indonesia. In addition, she is active as a research assistant at the Material Physics Laboratory, Faculty of Mathematics and Natural Sciences, University of Riau.